Johann Radon Institute for
Computational and Applied Mathematics
Austrian Academy of Sciences (ÖAW)

Detection and characterization of buried landmines using infrared thermography

T.T. Nguyen, H. Sahli, H. Dinh Nho

RICAM-Report 2011-25

Detection and characterization of buried landmines using infrared thermography*

Nguyen Trung Thành[1]† Hichem Sahli[2] and Dinh Nho Hào[3]
[1]Johann Radon Institute for Computational and Applied Mathematics (RICAM),
Austrian Academy of Sciences
Altenbergerstrasse 69, A-4040 Linz, Austria
Email: trung-thanh.nguyen@ricam.oeaw.ac.at
[2]Vrije Universiteit Brussel, Department of Electronics and Informatics,
Pleinlaan 2, 1050 Brussels, Belgium
Email: hsahli@etro.vub.ac.be
[3]Hanoi Institute of Mathematics, 18 Hoang Quoc Viet Road, 10307 Hanoi, Vietnam
Email: hao@math.ac.vn

Abstract

The application of infrared thermography to the detection and characterization of buried landmines (more generally, buried objects) is introduced. The problem is aimed at detecting the presence of objects buried under the ground and characterize them by estimating their thermal and geometrical properties using infrared measurements on the soil surface. Mathematically, this problem can be stated as an inverse problem for reconstructing a piecewise constant coefficient of a three-dimensional heat equation in a parallelepiped from only one measurement taken at one plane of its boundary (the air-soil interface). Due to the lack of spatial information in the observed data, this problem is extremely ill-posed. In order to reduce its ill-posedness, keeping in mind the application of detecting buried landmines, we make use of some simplification steps and propose a two-step method for solving it. The performance of the proposed algorithm is illustrated with numerical examples.

Keywords: infrared thermography, landmine detection, coefficient identification, heat equation, discrete adjoint method

AMS classification scheme numbers: 35K05, 35R05, 35R30, 80A23

1 Introduction

Thermal infrared (IR) technique has been applied to the detection of shallowly buried landmines for more than a decade and has been found to be promising for non-metallic mines. Its aim is to detect and distinguish landmines from other buried objects (false alarms) using diurnal IR measurements of the air-soil interface. The detection lies on the difference of the thermal characteristics between the soil and the buried objects. Indeed, the presence of buried objects affects the diurnal heat conduction inside the soil. Consequently, the soil temperature on the

*This paper was published in *Inverse problems in Science and Engineering*, vol. 19, no. 3, pp 281–307, 2011.
†Corresponding author

ground above the objects is often different from that of the background. This temperature can be measured by an IR imaging system placed above the soil area.

From measured thermal images, it is possible to detect the presence of shallowly buried anomalies using image processing techniques such as segmentation [4]. However, to classify these anomalies, one has to estimate their physical properties (thermal diffusivity), size and shape. Such a problem is often solved in two steps. The first step, referred to as *thermal modeling for shallowly buried objects*, aims at predicting the soil temperature provided that the thermal properties of the soil and the buried objects under investigation are known and given. In this step, a forward thermal model, which represents the physical theory of heat transfer processes inside the soil and on the soil surface, is established. In the second step, referred to as *inverse problem setting for landmine detection*, the forward thermal model and acquired IR images are used to detect the presence of buried objects and characterize them based on the estimation of their thermal and geometrical properties.

The forward thermal model helps understanding the effect of buried objects on the soil-surface thermal signatures while the inverse problem helps classifying the detected objects. So far, most of the works in IR technique for landmine detection have focused on defining and validating thermal models for buried landmines (see, e.g. [14, 23, 19, 25, 26]). However, there are just a few works considering the inverse problem [19, 25, 26]. Mathematically, the inverse problem is stated as the estimation of a piecewise constant coefficient of the heat equation from measurements on a surface of the boundary of the domain under investigation. There are two main difficulties in dealing with this problem: (i) it is extremely difficult to have a thermal model which is valid under different soil and weather conditions; (ii) the lack of spatial information in observed data since it is only taken at the air-soil interface while the coefficient needed to be estimated is a 3-D function. This is different from most of the publications on this topic in the literature in which the measured data is available on the whole boundary or even in the whole domain (see, e.g., [2, 7, 9, 11, 13, 17]).

Note that IR cameras do not measure the temperature of the soil surface itself but the thermal radiation emitted from the soil surface. In order to use the measured IR images in thermal modeling, a pre-processing chain, consisting of: 1) radiometric calibration; 2) temporal co-registration; 3) apparent temperature conversion; and 4) inverse perspective (ground) projection, must be applied. The output of this pre-processing chain is an image sequence of the soil-surface apparent temperature. A detailed description of the pre-processing steps is given in [4]. In this work, we consider the measured IR images as the soil-surface temperature measured during the period of analysis.

In [27] we proposed and validated a thermal model with the estimation of soil thermal properties from *in situ* measurements. This approach enables us to apply the thermal model in a wide range of soil and weather conditions, i.e. the first difficulty can be overcome. In this paper, we focus on surmounting the second difficulty of the inverse problem. For simplicity, we assume that there is only one buried object in the soil domain under investigation. Although this assumption is not always true in practice, in many cases it is possible to subdivide the soil area into small areas so that each of them contains only one object. This can be done using anomaly detection techniques [25]. We note that this assumption does not reduce the ill-posedness of the inverse problem. To further simplify the problem, keeping in mind our application of buried landmine detection, we assume that the buried object is an upright cylinder, but its horizontal cross-section is not necessarily circular. Under these assumptions, a buried object is specified by (i) its depth of burial, (ii) its height, (iii) its horizontal cross-section, and (iv) its thermal diffusivity. In this work we propose a two-step method for solving the inverse problem. In the

first step, we consider a given cross-section, and we estimate three parameters, namely, the depth of burial, the height, and the thermal diffusivity. This approach helps reducing the ill-posedness of the estimation problem as it reduces the number of unknown parameters. However, its result depends on the accuracy of the cross-section being given by the anomaly detection procedures. In the second step, we use the result of the previous step as an initial guess for estimating the full parameter vector, namely, the depth of burial, the height and the thermal diffusivity on a horizontal plane of the soil domain across the object. The cross-section is improved via the estimated thermal diffusivity on this plane. This step should improve the result of the first step.

In our approach, the inverse problem is stated as a least-squares minimization problem. To solve it, we make use of quasi-Newton trust region algorithm accompanied with discrete adjoint method for calculating the gradient of the objective functional and BFGS method for updating the Hessian of the objective functional. The performance of the algorithm is illustrated with some simulated numerical examples. More numerical results with real experimental data were reported in [29]. In that paper, we also analyzed the effects of several factors, e.g. the size of the object, its orientation (tilted cylinder), the uncertainty of the soil thermal diffusivity, on the identification results.

The paper is organized as follows: Section 2 is devoted to the mathematical formulation of the problem. In Section 3 we introduce a discrete inverse problem and formulate its gradient using the adjoint method. The two-step method for solving the inverse problem is presented in Section 4. Section 5 shows the performance of the proposed algorithms with some numerical examples. Finally, some conclusions are drawn in Section 6.

2 Mathematical statement of the problem

This section is devoted to the mathematical formulation of the inverse problem for landmine detection. To formulate the inverse problem, we make use of the forward thermal model which was introduced in [25, 27].

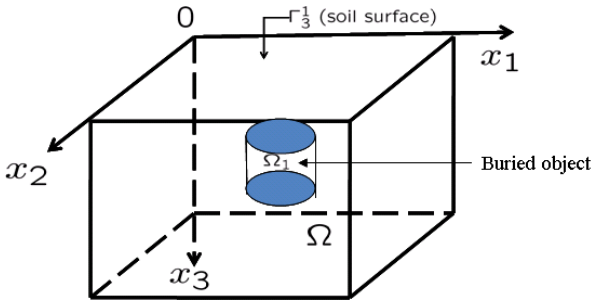

Figure 1: The soil volume with a buried object.

2.1 Forward thermal model

Consider an open rectangular parallelepiped Ω, which is composed of soil volume containing a buried object as shown in Figure 1. We associate the soil volume with an orthonormal Cartesian coordinate system in which the coordinate of a point is denoted by $x = (x_1, x_2, x_3)$. Without loss of generality, we assume that $\Omega = \{x : 0 < x_i < l_i,\ i = 1, 2, 3\}$. We denote by Γ the boundary of Ω and $\Gamma_i^1 = \{x \in \Gamma : x_i = 0\}$, $\Gamma_i^2 = \{x \in \Gamma : x_i = l_i\}$, $i = \overline{1,3}$. We note that Γ_3^1

is the air-soil interface (soil surface), the only portion of the soil volume accessible to thermal IR measurements, and Γ_3^2 is the bottom of the soil volume. For the simplicity of notation, the union of the vertical boundaries of Ω is denoted by $\Gamma_{1,2}$ ($\Gamma_{1,2} = (\Gamma \setminus \Gamma_3^1) \setminus \Gamma_3^2$). The duration of analysis is denoted by $(0, t_e)$ and $S_{i,t_e}^j := \Gamma_i^j \times (0, t_e)$, $i = 1, 2, 3,\ j = 1, 2$; $S_{t_e}^{1,2} := \Gamma_{1,2} \times (0, t_e)$. In this work, for simplicity, we assume that the soil and the object are isotropic and homogeneous, i.e. their thermal properties are constant. Moreover, the soil moisture content variation is assumed to be negligible during the period of analysis. Then the soil-temperature distribution $T(x,t),\ (x,t) \in \mathbb{Q}_{t_e} = \Omega \times (0, t_e)$, can be approximated by the following system [25]:

$$\begin{cases} \frac{\partial T}{\partial t}(x,t) - \sum_{i=1}^{3} \frac{\partial}{\partial x_i}\left(\alpha(x)\frac{\partial T(x,t)}{\partial x_i}\right) = 0,\ (x,t) \in \mathbb{Q}_{t_e}, \\ -\alpha(x)\frac{\partial T}{\partial x_3}(x,t) + pT(x,t) = q(t),\ (x,t) \in S_{3,t_e}^1, \\ T(x,t) = T_\infty,\ (x,t) \in S_{3,t_e}^2, \\ \frac{\partial T}{\partial n}(x,t) = 0,\ (x,t) \in S_{t_e}^{1,2}, \\ T(x,0) = g(x),\ x \in \Omega, \end{cases} \tag{1}$$

where $\alpha(x)$ (m^2/s) is the thermal diffusivity (of the soil and the buried object) in the domain. In this system, the first equation approximates the soil-temperature distribution inside the soil without external heat sources, the second one represents the heat flux at the air-soil interface due to convection and radiation, the third equation means that the soil temperature at a sufficiently deep depth is uniform (T_∞ is a constant), the fourth one is based on the assumption that the buried object does not disturb the soil around the vertical boundaries, the last one represents the distribution of the soil temperature at the beginning of the analysis. For the derivation of this model, we refer the reader to [25, 27].

Under the assumption that the soil and the buried object are homogeneous, the thermal diffusivity $\alpha(x)$ is described by a piecewise constant function

$$\alpha(x) = \begin{cases} \alpha_o,\ x \in \Omega_1, \\ \alpha_s,\ x \in \Omega \setminus \Omega_1. \end{cases}$$

Here α_s and α_o are the thermal diffusivity of the soil and the object, respectively; Ω_1 is the sub-domain of Ω occupied by the object.

In practical applications, it should be remarked that the bare-soil thermal diffusivity α_s, the boundary parameters p, $q(t)$ and the initial condition $g(x)$ are generally not available. In [27], we proposed methods for estimating these parameters from *in situ* measurements. In this paper, we therefore assume that these parameters are given.

It was proved in [25] that, under the hypothesis that $p > 0$, $q(t) \in H^1(0, t_e)$ and $g(x) \in H^1(\Omega)$, the forward thermal model (1) has a unique weak solution in the Sobolev space $H^{1,1}(\mathbb{Q}_{t_e})$, i.e. $T(x,t)$ belongs to the Sobolev space $H^{1,1}(\mathbb{Q}_{t_e})$ and satisfies the following system

$$\begin{cases} \int\limits_{\mathbb{Q}_{t_e}} T_t \eta dx dt + \int\limits_{\mathbb{Q}_{t_e}} \alpha T_x \eta_x dx dt + \int\limits_{S_{3,t_e}^1} pT\eta dx_3' dt = \int\limits_{S_{3,t_e}^1} q\eta dx_3' dt,\ \forall \eta \in \hat{H}^{1,0}(\mathbb{Q}_{t_e}), \\ T(x,t) = T_\infty,\ (x,t) \in S_{3,t_e}^2, \\ T(x,0) = g(x),\ x \in \Omega, \end{cases} \tag{2}$$

with $dx_3' = dx_1 dx_2$ and $\hat{H}^{1,0}(\mathbb{Q}_{t_e})$ being the subspace of $H^{1,0}(\mathbb{Q}_{t_e})$ consisting of all functions which vanish at the boundary S_{3,t_e}^2. Moreover, the weak solution satisfies the following energy

inequality:

$$\|T\|_{H^{1,1}(\mathbb{Q}_{t_e})} \leq C \left\{ \|q\|_{H^1(0,t_e)} + \|g\|_{H^1(\Omega)} + |T_\infty| \right\}, \tag{3}$$

where C is a positive constant independent of T.

In formulating the thermal model (1), we have assumed that the soil is isotropic and homogeneous and the soil surface is flat. This assumption, of course, is not always accurate. In a heat transfer process, when the temperature is rather high, the heat transfer characteristics usually depend on the temperature. However, in our case, the temperature is moderate, it is reasonable to suppose that these parameters are independent of the temperature. Of course, it is interesting to consider the case of temperature-depending coefficients but it is the subject of a future work. In addition, we only consider a small soil volume in our application, say, 50 cm by 50 cm by 50 cm around each object. Within such a small area, this assumption may be reasonable. The validity of the proposed forward problem for shallowly buried landmines was verified in [25, 27].

2.2 Statement of the inverse problem

Given the forward thermal model (2) (or, equivalently, (1)) and IR images measured at the air-soil interface, we now can state the inverse problem for landmine detection, i.e. estimating the thermal coefficient $\alpha(x)$ of the domain under consideration. It should be noted that the measured IR images can be considered as measured soil temperature at the air-soil interface, i.e. the boundary Γ_3^1 of the domain Ω. The estimation problem is aimed at finding $\alpha(x)$ such that the simulated soil-surface temperature using the forward model (2) fits the measured data. The most common way to set up this problem is the least-squares approach. Mathematically, it is equivalent to the following minimization problem

$$\min_{\alpha(x)} \mathcal{F}(\alpha) := \frac{1}{2} \int_0^{t_e} \int_{\Gamma_3^1} \left[T(x,t;\alpha) - \theta(x,t) \right]^2 dx_3' dt, \tag{4}$$

where $\theta(x,t)$ is the measured soil-surface temperature (IR images). Here we use the notation $T(x,t;\alpha)$ to emphasize the dependence of the solution to the forward problem (2) on the coefficient $\alpha(x)$.

We note that, since thermal properties of materials are positive and finite, the following bound constraints must be taken into account in solving the inverse problem (4) subject to (2)

$$0 < \alpha^l \leq \alpha(x) \leq \alpha^u, \ x \in \Omega, \tag{5}$$

where $[\alpha^l, \alpha^u]$ is the range to which the thermal diffusivity of the object is expected to belong.

2.3 On the existence and uniqueness

It is well-known that the coefficient estimation problem (4) subject to (2) and (5) may not have any solution unless the parameter space is properly chosen. The existence of a solution to the problem is guaranteed by the continuity of the objective functional $\mathcal{F}(\alpha)$ and the compactness of a subset of the parameter space to which the parameter belongs. In the literature, the parameter space may be chosen to be $H^1(\Omega)$ in order to guarantee the compactness of a bounded set in this space in $L_2(\Omega)$-norm [15, 16]. However, in this work, the coefficient $\alpha(x)$ is discontinuous in Ω. It does not belong to $H^1(\Omega)$ and therefore we have to look for it in another space. As

discussed in [9, 13], the space $BV(\Omega)$ of functions $f \in L_1(\Omega)$ of bounded variation in Ω ([8]) is a candidate. The next step is to find a set of functions satisfying the bound constraints (5) and is compact in $L_1(\Omega)$. To this end, we consider the set $\mathcal{K}_C$ which consists of all functions $\alpha(x) \in L_\infty(\Omega)$ satisfying (5) and their total variations are bounded by a constant $C > 0$. The compactness of $\mathcal{K}_C$ in L_1-norm was proved by Gutman [9].

On the other hand, it can be proved that the objective functional $\mathcal{F}(\alpha)$ is continuous from $L_1(\Omega)$ into $L_2(S^1_{3,t_e})$ (see [25]). Then we have the following existence result for the minimization problem.

Theorem 2.1. ***(Existence)*** *The minimization problem* (4) *subject to* (2) *has at least one solution in the subset* $\mathcal{K}_C$ *of the space* $BV(\Omega)$ *of functions of bounded variation.*

Although some results on the uniqueness of the coefficient identification problem have been published in the literature, most of the published works requires more than one (even infinitely many) measurements on the whole boundary or even in the whole domain for the coefficient to be uniquely determined, see, e.g., [7, 9, 10, 11]. Recently, the uniqueness for a one-dimensional coefficient estimation problem with piecewise constant coefficient and one measurement taken at one end of the one-dimensional rod was proved by Hoang and Ramm [12]. However, the technique used in the paper cannot be generalized to multidimensional cases. Moreover, for this problem, the main difficulty is due to the lack of spatial data as we want to determine the three-dimensional coefficient when only one measurement on a part of the boundary is given. Therefore, the uniqueness question is still open to us. For some simple cases, the analysis is under investigation.

3 Discretized inverse problem

To solve numerically the minimization problem (4) subject to (2), we make use of a quasi-Newton trust region algorithm proposed by Coleman and Li [3] with BFGS method for updating the Hessian of the objective functional. The algorithm has been implemented in the Matlab Optimization Toolbox in the function *fmincon* [22]. To calculate the gradient of the objective functional, the adjoint technique is widely used [18, 5, 6, 21, 24]. This technique helps calculating the gradient of the objective functional just by solving one forward problem and one adjoint problem. It is usually applied in the way that the adjoint problem of the forward model (2) is formulated, then both the objective functional and its gradient are approximated by discrete forms for numerical computations. The formulation of this approach is quite straightforward. However, many numerical trials have indicated that this approach might provide inaccurate approximates for the gradient of the objective functional, and even it might not converge at all [30, 1]. In this work, we therefore apply the technique in another way. That is, we first discretize the forward model and formulate the discrete objective functional corresponding to the discrete forward model. Then its gradient is exactly calculated via the solution of the discrete forward model and its adjoint problem.

3.1 Numerical methods for the forward model

In this work, we apply a finite difference splitting scheme to the forward problem [20, 27]. We note that, other discretization techniques such as the finite element method can also be used. We divide the domain Ω into parallelepipeds by the planes $\{x_i = k_i h_i\}$, with $k_i = 0, 1, \ldots, N_i$; $h_i = l_i/N_i$. To simplify the notation, we set $x(k) = (k_1 h_1, k_2 h_2, k_3 h_3)'$, $k = (k_1, k_2, k_3)'$ and $\Delta h =$

$h_1h_2h_3$. We also denote by e_i the unit normal vector along the x_i-direction in $\mathbb{R}^3$, i.e. $e_1 = (1,0,0)'$ and so on. In the following, we need the following notations

$$\omega_i(k) = \{x \in \Omega : k_ih_i \le x_i \le (k_i+1)h_i, (k_j-0.5)\,h_j \le x_j \le (k_j+0.5)\,h_j,\ \forall j \ne i\},$$
$$\bar{\Omega}_i^- = \{k : 0 \le k_i \le N_i - 1,\ 0 \le k_j \le N_j,\ \forall j \ne i\}.$$

We define the following mean values of the coefficient $\alpha(x)$

$$\alpha_i^+(k) = \frac{1}{|\omega_i(k)|}\int\limits_{\omega_i(k)} \alpha(x)dx,\ k \in \bar{\Omega}_i^-,$$

where $|\omega_i(k)|$ denotes the volume of $\omega_i(k)$. We also denote by $\alpha_i^-(k) := \alpha_i^+(k-e_i)$. The interval $[0,t_e]$ is divided into N_t equal sub-intervals by the points $t_i,\ i = \overline{0,N_t}:\ 0 = t_0 \le t_1 = \Delta t \le t_2 = 2\Delta t \le \cdots \le t_{N_t} = t_e$. We denote by $T^n(k)$ an approximate value of $T(x(k),t_n)$ and $T^n = \{T^n(k),\ k \in \bar{\Omega}_3^-\}$. The symbols $T^n_{x_i}$ and $T^n_{\bar{x}_i}$ denote the forward and backward finite difference quotients of T^n, respectively. In [27], using discrete approximations of the first equation of (2), we proposed the following finite difference splitting scheme

$$\begin{cases} T^0 = g^h, \\ (E_1 + \Delta t\mathcal{A}_1)T^{n+\frac{1}{3}} = T^n, \\ (E_2 + \Delta t\mathcal{A}_2)T^{n+\frac{2}{3}} = T^{n+\frac{1}{3}}, \\ (E_3 + \Delta t\mathcal{A}_3)T^{n+1} = T^{n+\frac{2}{3}} + \Delta tF^{n+\frac{1}{2}}, \end{cases} \tag{6}$$

for $n = \overline{0,N_t-1}$ with $g^h(k) = g(x(k))$, and the operators defined by

$$(\mathcal{A}_1T^n)(k) = \begin{cases} \frac{\alpha_1^-(k)T^n_{\bar{x}_1}(k)}{h_1} - \frac{\alpha_1^+(k)T^n_{x_1}(k)}{h_1},\ 1 \le k_1 \le N_1 - 1, \\ -\frac{\alpha_1^+(k)}{h_1}T^n_{x_1}(k),\ k_1 = 0, \\ \frac{\alpha_1^-(k)}{h_1}T^n_{\bar{x}_1}(k),\ k_1 = N_1. \end{cases} \tag{7}$$

$$(\mathcal{A}_2T^n)(k) = \begin{cases} \frac{\alpha_2^-(k)T^n_{\bar{x}_2}(k)}{h_2} - \frac{\alpha_2^+(k)T^n_{x_2}(k)}{h_2},\ 1 \le k_2 \le N_2 - 1, \\ -\frac{\alpha_2^+(k)T^n_{x_2}(k)}{h_2},\ k_2 = 0, \\ \frac{\alpha_2^-(k)T^n_{\bar{x}_2}(k)}{h_2},\ k_2 = N_2. \end{cases} \tag{8}$$

$$(\mathcal{A}_3T^n)(k) = \begin{cases} \frac{\alpha_3^-(k)T^n_{\bar{x}_3}(k)}{h_3} - \frac{\alpha_3^+(k)T^n_{x_3}(k)}{h_3},\ 1 \le k_3 \le N_3 - 2, \\ -\frac{\alpha_3^+(k)T^n_{x_3}(k)}{h_3} + \frac{pT^n(k)}{h_3},\ k_3 = 0, \\ \frac{\alpha_3^-(k)T^n_{\bar{x}_3}(k)}{h_3} + \frac{\alpha_3^+(k)T^n(k)}{h_3^2},\ k_3 = N_3 - 1. \end{cases} \tag{9}$$

The symbol E_i denotes the identity matrix associated with $\mathcal{A}_i,\ i = \overline{1,3}$. Finally, the matrix $F^{n+\frac{1}{2}}$ is given by

$$F^{n+\frac{1}{2}}(k) = \begin{cases} \frac{q(t_n)+q(t_{n+1})}{2h_3}, & \text{if } k_3 = 0, \\ \frac{\alpha_3^+(k)T_\infty}{h_3^2}, & \text{if } k_3 = N_3 - 1, \\ 0 & \text{otherwise.} \end{cases} \tag{10}$$

It was proved that the above splitting scheme converges to the unique solution of (2) [27, 25]. Moreover, this scheme is absolutely stable and faster than other implicit schemes and its implementation is simple.

3.2 Discrete minimization problem

In the sequel, we consider (6) as the discrete forward model for shallowly buried objects. Corresponding to this model, the objective functional (4) is replaced by the following discrete one:

$$\mathcal{F}_h(\alpha) := \frac{\Delta t h_1 h_2}{2} \sum_{n=0}^{N_t} \sum_{k \in \Gamma_{3h}^1} \left[T^n(k;\alpha) - \theta^n(k_1,k_2)\right]^2, \tag{11}$$

with $\left\{T^n(k;\alpha),\ k \in \bar{\Omega}_3^-,\ n = \overline{0,N_t}\right\}$ being the solution of the discrete forward problem (6) associated with the coefficient $\alpha(x)$ and $\left\{\theta^n(k_1,k_2),\ 0 \le k_i \le N_i,\ n = \overline{0,N_t}\right\}$ being the measured soil-surface temperature at the space and time grid nodes. Here, Γ_{3h}^1 represents the set of grid points on the soil-surface. It is clear that the discrete objective functional $\mathcal{F}_h(\alpha)$ is an approximation of the continuous one.

It should be noted that, in the discrete problem, the coefficient $\alpha(x),\ x \in \Omega$, can be replaced by the average values $\alpha_i^+(k),\ k \in \bar{\Omega}_3^-,\ i = \overline{1,3}$. For shortening the notation, in the following, we denote by $\alpha_i(k) := \alpha_i^+(k)$ and $\alpha_i := \{\alpha_i(k),\ k \in \bar{\Omega}_3^-\}$. Since $\alpha(x)$ is bounded by (5), the average values $\alpha_i(k)$ are also bounded by

$$0 < \alpha^l \le \alpha_i(k) \le \alpha^u,\ k \in \bar{\Omega}_3^-,\ i = \overline{1,3}. \tag{12}$$

For each $i = \overline{1,3}$, it is clear from (7)–(9) that the coefficient matrix $\mathcal{A}_i$ depends on (and only on) α_i (in the following, we sometimes use the notation $\mathcal{A}_i(\alpha_i)$ to emphasize the dependence of $\mathcal{A}_i$ on α_i). Moreover, F is a function of $\alpha_3(k)$ for $k_3 = N_3 - 1$. For simplicity, we assume that the object is shallowly buried, so the deep layers consist of only homogeneous soil. Under this assumption, we have $\alpha_3(k) = \alpha_s$ for $k_3 = N_3 - 1$. Therefore, $F^{n+\frac{1}{2}}(k)$ does not depend on the unknown coefficient. Moreover, with the assumption that the object is so small that the vertical boundary layers of the soil domain contain only homogeneous soil, we have that $\alpha_i(k) = \alpha_s$ at the vertical boundary points, e.g. for $k_1 = 0$ or $k_1 = N_1$. Hence, we only need to consider the variables $\alpha_i(k)$ for $1 \le k_1 \le N_1 - 1$, $1 \le k_2 \le N_2 - 1$, $0 \le k_3 \le N_3 - 2$. This assumption helps reducing the complexity of the numerical implementation.

We also note that the discrete forward model (6) can be rewritten as

$$\begin{cases} \mathcal{A}(\alpha)T^{n+1} - T^n = \Delta t \mathcal{C}(\alpha) F^{n+\frac{1}{2}},\ n = \overline{0,N_t-1}, \\ T^0 = g^h, \end{cases} \tag{13}$$

where

$$\begin{aligned} \mathcal{A}(\alpha) &= \left(E_1 + \Delta t \mathcal{A}_1(\alpha_1)\right)\left(E_2 + \Delta t \mathcal{A}_2(\alpha_2)\right)\left(E_3 + \Delta t \mathcal{A}_3(\alpha_3)\right), \\ \mathcal{C}(\alpha) &= \left(E_1 + \Delta t \mathcal{A}_1(\alpha_1)\right)\left(E_2 + \Delta t \mathcal{A}_2(\alpha_2)\right). \end{aligned}$$

By considering the average values of the coefficient $\alpha(x)$ as the unknown parameters, the parameter space in this case is finite dimensional. Hence, the subset of the unknown parameters satisfying the constraints (12) is compact in this space. Moreover, we will prove in the next section that the objective function (11) is differentiable. Thus, the discrete optimization problem has at least one solution. We state this property in the following theorem.

Theorem 3.1. *The discrete optimization problem* (11) *subject to* (6) *and* (12) *has at least one solution.*

3.3 Gradient of the discrete objective functional

The objective of this section is to calculate the gradient of the discrete objective functional (11). To this end, we consider an infinitesimal variation $\delta\alpha$ of the coefficient α. By denoting $\alpha'(x) = \alpha(x) + \delta\alpha(x)$ and $\alpha_i'(k) = \alpha_i(k) + \delta\alpha_i(k)$, we have from (11) that

$$\begin{aligned}
\mathcal{F}_h(\alpha') - \mathcal{F}_h(\alpha) &= \frac{\Delta t h_1 h_2}{2} \sum_{n=0}^{N_t} \sum_{k_1=0}^{N_1} \sum_{k_2=0}^{N_2} \left[T^n(k_1,k_2,0;\alpha') - \theta^n(k_1,k_2)\right]^2 \\
&\quad - \frac{\Delta t h_1 h_2}{2} \sum_{n=0}^{N_t} \sum_{k_1=0}^{N_1} \sum_{k_2=0}^{N_2} \left[T^n(k_1,k_2,0;\alpha) - \theta^n(k_1,k_2)\right]^2 \\
&= \frac{\Delta t h_1 h_2}{2} \sum_{n=0}^{N_t} \sum_{k_1=0}^{N_1} \sum_{k_2=0}^{N_2} \left[U^n(k_1,k_2,0)\right]^2 \\
&\quad + \Delta t h_1 h_2 \sum_{n=0}^{N_t} \sum_{k_1=0}^{N_1} \sum_{k_2=0}^{N_2} U^n(k_1,k_2,0) \left[T^n(k_1,k_2,0;\alpha) - \theta^n(k_1,k_2)\right],
\end{aligned} \tag{14}$$

where $U^n(k) = T^n(k;\alpha') - T^n(k;\alpha),\ n = \overline{0, N_t - 1},\ k \in \bar{\Omega}_3^-$. It follows from (13) that $U := \{U^n(k),\ n = \overline{0, N_t - 1},\ k \in \bar{\Omega}_3^-\}$ is the solution of the following problem

$$\begin{cases} \left[\mathcal{A}(\alpha)U^{n+1}\right](k) - U^n(k) = \Delta t \left[\delta\mathcal{C}(\alpha)F^{n+\frac{1}{2}}\right](k) - \left[\delta\mathcal{A}(\alpha)T^{n+1}\right](k,\alpha'),\ k \in \bar{\Omega}_3^-,\ n = \overline{0, N_t - 1}, \\ U^0 = 0, \end{cases}$$

where $\delta\mathcal{C}(\alpha) = \mathcal{C}(\alpha') - \mathcal{C}(\alpha)$ and $\delta\mathcal{A}(\alpha) = \mathcal{A}(\alpha') - \mathcal{A}(\alpha)$. Consider an arbitrary matrix $\eta = \{\eta^n(k),\ n = \overline{0, N_t - 1},\ k \in \bar{\Omega}_3^-\}$. Multiplying both sides of the first equation by $\eta^n(k)$, summing up the results with respect to $k \in \bar{\Omega}_3^-$ and $n = \overline{1, N_t - 1}$, we have

$$\begin{aligned}
&\sum_{n=0}^{N_t-1} \sum_{k\in\bar{\Omega}_3^-} \left[\mathcal{A}(\alpha)U^{n+1}\right](k)\eta^{n+1}(k) - \sum_{n=0}^{N_t-1} \sum_{k\in\bar{\Omega}_3^-} U^n(k)\eta^{n+1}(k) \\
&= \Delta t \sum_{n=0}^{N_t-1} \sum_{k\in\bar{\Omega}_3^-} \left[\delta\mathcal{C}(\alpha)F^{n+\frac{1}{2}}\right](k)\eta^{n+1}(k) - \sum_{n=0}^{N_t-1} \sum_{k\in\bar{\Omega}_3^-} \left[\delta\mathcal{A}(\alpha)T^{n+1}\right](k,\alpha')\eta^{n+1}(k).
\end{aligned}$$

If η satisfies the following equation

$$\begin{aligned}
&\sum_{n=0}^{N_t-1} \sum_{k\in\bar{\Omega}_3^-} \left[\mathcal{A}(\alpha)U^{n+1}\right](k)\eta^{n+1}(k) - \sum_{n=0}^{N_t-1} \sum_{k\in\bar{\Omega}_3^-} U^n(k)\eta^{n+1}(k) \\
&= \frac{1}{h_3} \sum_{n=0}^{N_t} \sum_{k_1=0}^{N_1} \sum_{k_2=0}^{N_2} U^n(k_1,k_2,0) \left[T^n(k_1,k_2,0;\alpha) - \theta^n(k_1,k_2)\right],
\end{aligned} \tag{15}$$

then the variation of the discrete objective functional is given by

$$\begin{aligned}\mathcal{F}_h(\alpha') - \mathcal{F}_h(\alpha) = \frac{\Delta t h_1 h_2}{2} \sum_{n=0}^{N_t} \sum_{k_1=0}^{N_1} \sum_{k_2=0}^{N_2} [U^n(k_1,k_2,0)]^2 \\ + \Delta t^2 \Delta h \sum_{n=0}^{N_t-1} \sum_{k\in\bar{\Omega}_3^-} \left[\delta\mathcal{C}(\alpha) F^{n+\frac{1}{2}}\right](k)\eta^{n+1}(k) \\ - \Delta t \Delta h \sum_{n=0}^{N_t-1} \sum_{k\in\bar{\Omega}_3^-} \left[\delta\mathcal{A}(\alpha) T^{n+1}\right](k,\alpha')\eta^{n+1}(k).\end{aligned} \tag{16}$$

Before deriving the gradient of $\mathcal{F}_h(\alpha)$, let us first define the discrete adjoint problem from (15). Suppose that $\xi = \left\{\xi^n(k),\ k \in \bar{\Omega}_3^-,\ n = \overline{0, N_t}\right\}$ is specified by

$$\xi^n(k) = \begin{cases} \frac{1}{h_3}\left[T^n(k;\alpha) - \theta^n(k_1,k_2)\right] & \text{if } k_3 = 0, \\ 0 & \text{otherwise,} \end{cases} \tag{17}$$

then we have from (15) the following discrete adjoint problem

$$\begin{cases} \mathcal{A}^*(\alpha)\eta^n - \eta^{n+1} = \xi^n,\ n = N_t - 1, N_t - 2, \ldots, 2, \\ \mathcal{A}^*(\alpha)\eta^{N_t} = \xi^{N_t}, \end{cases} \tag{18}$$

with $\mathcal{A}^*(\alpha)$ being the adjoint operator of $\mathcal{A}(\alpha)$. Since the matrices A_i, $i = 1, 2, 3$, are positive semi-definite and symmetric as proved in [27], we have

$$A^*(\alpha) = (E_3 + \Delta t \mathcal{A}_3)(E_2 + \Delta t \mathcal{A}_2)(E_1 + \Delta t \mathcal{A}_1).$$

With the above representation of the operator $\mathcal{A}^*(\alpha)$, the discrete adjoint problem can be rewritten in the following form

- For $n = N_t$:

$$\begin{cases} (E_3 + \Delta t \mathcal{A}_3)\eta^{N_t+\frac{2}{3}} = \xi^{N_t}, \\ (E_2 + \Delta t \mathcal{A}_2)\eta^{N_t+\frac{1}{3}} = \eta^{N_t+\frac{2}{3}}, \\ (E_1 + \Delta t \mathcal{A}_1)\eta^{N_t} = \eta^{N_t+\frac{1}{3}}. \end{cases}$$

- For $n = N_t - 1, N_t - 2, \ldots, 2$:

$$\begin{cases} (E_3 + \Delta t \mathcal{A}_3)\eta^{n+\frac{2}{3}} = \xi^n + \eta^{n+1}, \\ (E_2 + \Delta t \mathcal{A}_2)\eta^{n+\frac{1}{3}} = \eta^{n+\frac{2}{3}}, \\ (E_1 + \Delta t \mathcal{A}_1)\eta^{n} = \eta^{n+\frac{1}{3}}. \end{cases}$$

This problem is solved in a similar way as the discrete forward model (6).

We now turn back to the gradient of the discrete objective functional. We can prove by induction that [28]

$$\frac{\Delta t h_1 h_2}{2} \sum_{n=0}^{N_t} \sum_{k_1=0}^{N_1} \sum_{k_2=0}^{N_2} [U^n(k_1,k_2,0)]^2 = o(\delta\alpha). \tag{19}$$

We also have

$$\begin{aligned}\delta\mathcal{C}(\alpha) &= [E_1 + \Delta t\mathcal{A}_1(\alpha_1')][E_2 + \Delta t\mathcal{A}_2(\alpha_2')] - [E_1 + \Delta t\mathcal{A}_1(\alpha_1)][E_2 + \Delta t\mathcal{A}_2(\alpha_2)] \\ &= \Delta t\delta\mathcal{A}_1(\alpha_1)[E_2 + \Delta t\mathcal{A}_2(\alpha_2')] + \Delta t[E_1 + \Delta t\mathcal{A}_1(\alpha_1)]\delta\mathcal{A}_2(\alpha_2),\end{aligned}$$

with $\delta\mathcal{A}_i(\alpha_i) = \mathcal{A}_i(\alpha_i') - \mathcal{A}_i(\alpha_i)$. We note that $F^{n+\frac{1}{2}}(k)$ does not depend on either the coefficient $\alpha(x)$ or the values of k_1 and k_2. Therefore, $\mathcal{A}_1F^{n+\frac{1}{2}}(k) = 0$ and $\mathcal{A}_2F^{n+\frac{1}{2}}(k) = 0$ for $k \in \bar{\Omega}_3^-$. By elementary arguments, we also have that $\delta C(\alpha)F^{n+\frac{1}{2}} = 0$. From these equalities, (16) and (19), the variation of the objective functional can be rewritten as

$$\mathcal{F}_h(\alpha') - \mathcal{F}_h(\alpha) = -\Delta t\Delta h\sum_{n=1}^{N_t}\sum_{k\in\bar{\Omega}_3^-}\left(\delta\mathcal{A}(\alpha)T^n\right)(k,\alpha')\eta^n(k) + o(\delta\alpha). \tag{20}$$

The variation $\delta\mathcal{A}(\alpha)$ can be represented by

$$\delta\mathcal{A}(\alpha) = \delta\mathcal{A}^1(\alpha) + \delta\mathcal{A}^2(\alpha) + \delta\mathcal{A}^3(\alpha),$$

where

$$\begin{aligned}\delta\mathcal{A}^1(\alpha) &= \Delta t\delta\mathcal{A}_1(\alpha_1)\left[E_2 + \Delta t\mathcal{A}_2(\alpha_2')\right][E_3 + \Delta t\mathcal{A}_3(\alpha_3')], \\ \delta\mathcal{A}^2(\alpha) &= \Delta t[E_1 + \Delta t\mathcal{A}_1(\alpha_1)]\delta\mathcal{A}_2(\alpha_2)[E_3 + \Delta t\mathcal{A}_3(\alpha_3')], \\ \delta\mathcal{A}^3(\alpha) &= \Delta t[E_1 + \Delta t\mathcal{A}_1(\alpha_1)][E_2 + \Delta t\mathcal{A}_2(\alpha_2)]\delta\mathcal{A}_3(\alpha_3).\end{aligned}$$

From (7)–(9) we have that for each $i \in \{1,2,3\}$, the coefficient matrix $\mathcal{A}_i$ is continuous in α_i, so $\mathcal{A}_i(\alpha_i')$ converges to $\mathcal{A}_i(\alpha_i)$ as $\delta\alpha$ tends to zero. To derive the gradient of the objective functional, it is sufficient to formulate the directional derivatives of $\mathcal{A}_i(\alpha_i)T^n$ with respect to $\alpha_i(k)$. For $k \in \bar{\Omega}_3^- :\ 1 \le k_1 \le N_1 - 1$, we have

$$\begin{aligned}\left[\delta\mathcal{A}^1(\alpha)T^n\right](k) = &\frac{\Delta t}{h_1}\left([E_2 + \Delta t\mathcal{A}_2(\alpha_2')][E_3 + \Delta t\mathcal{A}_3(\alpha_3')]T^n\right)_{\bar{x}_1}(k)\delta\alpha_1(k-e_1) \\ &- \frac{\Delta t}{h_1}\left([E_2 + \Delta t\mathcal{A}_2(\alpha_2')][E_3 + \Delta t\mathcal{A}_3(\alpha_3')]T^n\right)_{x_1}(k)\delta\alpha_1(k).\end{aligned}$$

Therefore,

$$\frac{\partial[\mathcal{A}^1(\alpha_1)T^n](m)}{\partial\alpha_1(k)} = \begin{cases} -\frac{\Delta t}{h_1}\left([E_2 + \Delta t\mathcal{A}_2(\alpha_2')][E_3 + \Delta t\mathcal{A}_3(\alpha_3')]T^n\right)_{x_1}(k) & \text{if } m = k, \\ \frac{\Delta t}{h_1}\left([E_2 + \Delta t\mathcal{A}_2(\alpha_2')][E_3 + \Delta t\mathcal{A}_3(\alpha_3')]T^n\right)_{x_1}(k) & \text{if } m = k + e_1, \\ 0 & \text{otherwise.}\end{cases} \tag{21}$$

Since $\mathcal{A}_2$ and $\mathcal{A}_3$ do not depend on α_1, taking the limit as $\delta\alpha_1$ tends to zero, we have from (20) and (21) that

$$\begin{aligned}\frac{\partial\mathcal{F}_h}{\partial\alpha_1(k)} &= -\Delta t\Delta h\sum_{n=1}^{N_t}\sum_{m\in\bar{\Omega}_3^-}\frac{\partial\left[\left(\mathcal{A}^1T^n\right)(m)\right]}{\partial\alpha_1(k)}\eta^n(m) \\ &= -\Delta t\Delta h\sum_{n=1}^{N_t}\left\{\frac{\partial\left[\left(\mathcal{A}^1T^n\right)(k)\right]}{\partial\alpha_1(k)}\eta^n(k) + \frac{\partial\left[\left(\mathcal{A}^1T^n\right)(k+e_1)\right]}{\partial\alpha_1(k)}\eta^n(k+e_1)\right\} \qquad (22) \\ &= -\Delta t^2\Delta h\sum_{n=1}^{N_t}\left[(E_2 + \Delta t\mathcal{A}_2)(E_3 + \Delta t\mathcal{A}_3)T^n\right]_{x_1}(k)\eta_{x_1}^n(k).\end{aligned}$$

Denoting by $\mu_i = \Delta t/h_i^2,\ i = 1, 2, 3$, we obtain, for $1 \le k_2 \le N_2 - 1,\ 1 \le k_3 \le N_3 - 2$,

$$\begin{aligned}
&[(E_2 + \Delta t\mathcal{A}_2)(E_3 + \Delta t\mathcal{A}_3)T^n](k) = \\
&- \mu_2\alpha_2(k - e_2)[T^n(k - e_2) + \mu_3\alpha_3(k - e_2 - e_3)h_3T^n_{\bar{x}_3}(k - e_2) - \mu_3\alpha_3(k - e_2)h_3T^n_{x_3}(k - e_2)] \\
&+ [1 + \mu_2(\alpha_2(k - e_2) + \alpha_2(k))]\,[T^n(k) + \mu_3\alpha_3(k - e_3)h_3T^n\bar{x}_3(k) - \mu_3\alpha_3(k)h_3T^n_{x_3}(k)] \\
&- \mu_2\alpha_2(k)[T^n(k + e_2) + \mu_3\alpha_3(k + e_2 - e_3)h_3T^n_{\bar{x}_3}(k + e_2) - \mu_3\alpha_3(k + e_2)h_3T^n_{x_3}(k + e_2)].
\end{aligned} \tag{23}$$

Similarly, for $1 \le k_2 \le N_2 - 1,\ k_3 = 0$, we have

$$\begin{aligned}
&[(E_2 + \Delta t\mathcal{A}_2)(E_3 + \Delta t\mathcal{A}_3)T^n](k) = \\
&- \mu_2\alpha_2(k - e_2)\,\{(1 + \mu_3ph_3)T^n(k - e_2) - \mu_3\alpha_3(k - e_2)[T^n(k - e_2 + e_3) - T^n(k - e_2)]\} \\
&+ [1 + \mu_2(\alpha_2(k - e_2) + \alpha_2(k))]\,\{(1 + \mu_3ph_3)T^n(k) - \mu_3\alpha_3(k)[T^n(k + e_3) - T^n(k)]\} \\
&- \mu_2\alpha_2(k)\{(1 + \mu_3ph_3)T^n(k + e_2) - \mu_3\alpha_3(k + e_2)[T^n(k + e_2 + e_3) - T^n(k + e_2)]\}.
\end{aligned} \tag{24}$$

The directional derivatives of the objective functional with respect to $\alpha_1(k)$, $1 \le k_1 \le N_1 - 1,\ 1 \le k_2 \le N_2 - 1,\ 0 \le k_3 \le N_3 - 2$, are calculated using (22)–(24). The derivatives of $\mathcal{F}_h$ with respect to $\alpha_2(k)$ and $\alpha_3(k)$ are given by similar formulae. For more details, we refer the reader to [25].

4 Simplifications of the inverse problem

The optimization problem (11) subject to (6) and (12) for estimating the coefficient $\alpha(x)$ is severely ill-posed due to the lack of spatial information in the measured data. Numerical tests have indicated that it is difficult to obtain reliable estimates unless more constraints or simplifications are used. The choice of the constraints or simplifications depends on particular applications. As our objective is to detect landmines and distinguish them from other false alarms, we assume that the buried objects to be reconstructed are cylinders but, for generality, their cross-sections are not necessarily circular. Moreover, they are upright buried. Under these assumptions, a buried object is specified by (i) depth of burial, (ii) height, (iii) horizontal cross-section, and (iv) thermal diffusivity. In this work we propose a two-step method for solving the inverse problem. In the first step, we consider a given cross-section, and we estimate three parameters, namely, the depth of burial, the height, and the thermal diffusivity. This approach helps reducing the ill-posedness of the estimation problem as it reduces dramatically the number of unknown parameters (only three parameters are to be reconstructed). However, its result depends on the accuracy of the cross-section being given by anomaly detection procedures [25].

In the second step, we reconstruct the full parameter vector, namely, the depth of burial, the height and the mean values of the thermal diffusivity on a horizontal plane of the soil domain across the object. Since this problem is severely ill-posed, we need a good initial guess in order to obtain a reasonable estimate. For this purpose, the result of the previous step is used. The cross-section is improved via the estimated mean values of the thermal diffusivity. This step should improve the result of the first step. In the following, we refer the first and the second steps as *Step* 1 and *Step* 2, respectively.

With the assumption of cylindrical shape of the object, we can represent the coefficient $\alpha(x)$ as follows

$$\alpha(x) = \begin{cases} \alpha_{12}(x_1, x_2), \text{ if } \varrho_1 \le x_3 \le \varrho_2, \\ \alpha_s, \text{ otherwise,} \end{cases} \tag{25}$$

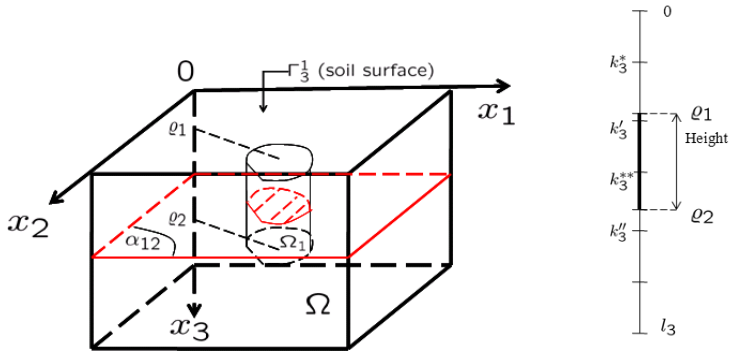

(a) (b)

Figure 2: (a) Horizontal cross-section of the soil domain across the object; (b) The location of the object in depth.

where ϱ_1 and ϱ_2 are the locations of the top and the bottom surfaces of the object in the soil volume ($0 < \varrho_1 < \varrho_2 < l_3$), and $\alpha_{12}(x_1, x_2)$, $0 \le x_i \le l_i$, $i = 1, 2$, is the coefficient on a horizontal surface of the soil domain across the object (Figure 2(a)). For simplicity, we assume that the height of the object is not less than the corresponding grid size, that is, $\varrho_2 - \varrho_1 \ge h_3$. Furthermore, if we denote by $\gamma_{3i}^1(k_1, k_2)$ the projection of $\omega_i(k)$ on the surface Γ_3^1, and $\alpha_{12}^i(k_1, k_2)$, $1 \le k_i \le N_i - 1$, $i = 1, 2, 3$, specified by

$$\alpha_{12}^i(k_1, k_2) = \frac{1}{h_1 h_2} \int\limits_{\gamma_{3i}^1(k_1,k_2)} \alpha_{12}(x_1, x_2) dx_1 dx_2$$

and suppose that the location of the top surface of the object falls into the grid intervals $[(k_3' - 0.5)h_3, (k_3' + 0.5)h_3)$ and $[k_3^* h_3, (k_3^* + 1)h_3)$, while the bottom surface falls into the intervals $[(k_3'' - 0.5)h_3, (k_3'' + 0.5)h_3)$ and $[k_3^{**} h_3, (k_3^{**} + 1)h_3)$ (see Figure 2(b)). That is,

$$\begin{aligned} &(k_3' - 0.5)h_3 \le \varrho_1 < (k_3' + 0.5)h_3, \quad (k_3'' - 0.5)h_3 \le \varrho_2 < (k_3'' + 0.5)h_3, \\ &k_3^* h_3 \le \varrho_1 < (k_3^* + 1)h_3, \quad k_3^{**} h_3 \le \varrho_2 < (k_3^{**} + 1)h_3, \end{aligned}$$

then the average values $\alpha_i(k)$, $1 \le k_1 \le N_1 - 1$, $1 \le k_2 \le N_2 - 1$, $0 \le k_3 \le N_3 - 2$, can be represented as

$$\alpha_i(k) = \begin{cases} \alpha_s, \text{ if } k_3 < k_3', \\ \frac{1}{h_3}\left\{\alpha_s[\varrho_1 - (k_3' - 0.5)h_3] + \alpha_{12}^i(k_1, k_2)[(k_3' + 0.5)h_3 - \varrho_1]\right\}, \text{ if } k_3 = k_3', \\ \alpha_{12}^i(k_1, k_2), \text{ if } k_3' + 1 \le k_3 \le k_3'' - 1, \\ \frac{1}{h_3}\left\{\alpha_{12}^i(k_1, k_2)[\varrho_2 - (k_3'' - 0.5)h_3] + \alpha_s[(k_3'' + 0.5)h_3 - \varrho_2]\right\}, \text{ if } k_3 = k_3'', \\ \alpha_s, \text{ if } k_3 > k_3'', \end{cases}$$

for $i = 1, 2$ and

$$\alpha_3(k) = \begin{cases} \alpha_s, \text{ if } k_3 < k_3^*, \\ \frac{1}{h_3}\left\{\alpha_s[\varrho_1 - k_3^* h_3] + \alpha_{12}^3(k_1, k_2)[(k_3^* + 1)h_3 - \varrho_1]\right\}, \text{ if } k_3 = k_3^*, \\ \alpha_{12}^3(k_1, k_2), \text{ if } k_3^* + 1 \le k_3 \le k_3^{**} - 1, \\ \frac{1}{h_3}\left\{\alpha_{12}^3(k_1, k_2)[\varrho_2 - k_3^{**} h_3] + \alpha_s[(k_3^{**} + 1)h_3 - \varrho_2]\right\}, \text{ if } k_3 = k_3^{**}, \\ \alpha_s, \text{ if } k_3 > k_3^{**}. \end{cases}$$

If we consider the average values $\alpha_{12}^i(k_1,k_2),\ 1\le k_1\le N_1-1,\ 1\le k_2\le N_2-1$, and $\varrho_1,\ \varrho_2$ as new variables, the derivatives of $\alpha_i,\ i=1,2$, with respect to these variables are given by

$$\frac{\partial\alpha_i(k)}{\partial\alpha_{12}^i(k_1,k_2)}=\begin{cases}\frac{1}{h_3}[(k_3'+0.5)h_3-\varrho_1],\ \text{if } k_3=k_3',\\ \frac{1}{h_3}[\varrho_2-(k_3''-0.5)h_3],\ \text{if } k_3=k_3'',\\ 1,\ \text{if } k_3'+1\le k_3\le k_3''-1,\\ 0,\ \text{otherwise.}\end{cases}$$

$$\frac{\partial\alpha_i(k)}{\partial\varrho_1}=\begin{cases}\frac{1}{h_3}[\alpha_s-\alpha_{12}^i(k_1,k_2)],\ \text{if } k_3=k_3',\\ 0,\ \text{otherwise.}\end{cases}$$

$$\frac{\partial\alpha_i(k)}{\partial\varrho_2}=\begin{cases}\frac{1}{h_3}[\alpha_{12}^i(k_1,k_2)-\alpha_s],\ \text{if } k_3=k_3'',\\ 0,\ \text{otherwise.}\end{cases}$$

Similar formulae are obtained for α_3. Using the chain rule, we have the derivatives of the objective functional $\mathcal{F}_h$ with respect to the new variables $\alpha_{12}^i(k_1,k_2),\ 1\le k_1\le N_1-1,\ 1\le k_2\le N_2-1,\ i=1,2,3$, and $\varrho_1,\ \varrho_2$. Finally, the height of the object is given by $\varsigma=\varrho_2-\varrho_1$.

In solving the estimation problem, some constraints of the unknown parameters must be taken into account. It is obvious that the average values $\alpha_{12}^i(k)$ are bounded by α^l and α^u as in (12), i.e.

$$0<\alpha^l\le\alpha_{12}^i\le\alpha^u. \tag{26}$$

We also remark that, as analyzed in [25], the detection can only be possible for shallowly buried objects, say, at most 10-cm deep for common anti-personnel (AP) mines. Hence, the depth of burial ϱ_1 should not be too large. Moreover, since we assume that the soil-surface contains only homogeneous soil, the depth of burial must be positive. More precisely, we have

$$0<\varrho_1^l\le\varrho_1\le\varrho_1^u<l_3, \tag{27}$$

where d_1^l is a small positive value which prevents the depth of burial from converging to zero and d_1^u is the maximum depth of burial at which the object is still detectable.

Concerning the height of the object, we have indicated in [25] that the effect of the object's height on the soil-surface temperature contrast is very small. The contrasts associated with two values of the height are still distinguishable only if these values do not greater than a certain threshold (e.g. approximately 5 cm for common AP mines). Hence, an estimated value of the height is reliable only in this range, i.e. the following constraints should be added to the estimation problem

$$h_3\le\varsigma\le\varsigma^u, \tag{28}$$

where ς^u is the maximum height of the object at which the estimation is still reliable. Note that this parameter must be chosen so that $\varrho_1^u+\varsigma^u<l_3$.

4.1 Cylindrical object with the given cross section

Our first idea is to reduce the ill-posedness of the inverse problem by applying image segmentation techniques to estimate the cross-section of the buried object and hence reduce the number of unknown parameters. Image segmentation techniques help detecting the presence of an anomaly in an image sequence and provides a rough estimate of its horizontal size and shape. The result

is a binary mask corresponding to the location and the shape of the anomaly, i.e. the (approximate) cross-section of the buried object. The inverse problem is then reduced to estimate only three parameters: the thermal diffusivity, the depth of burial and the height of the object.

In [29] we developed a segmentation technique for both detecting the presence of anomalies and estimating their sizes. The method makes use of a threshold criterion for the soil-surface temperature contrast which is based on its dependence on the depth, size and thermal diffusivity of the object. For more details, we refer to [29]. Here we assume that $\tilde{\Gamma}_3^1$ is the estimated cross-section of the buried object. With the estimated cross-section and the assumption that the buried object is homogeneous, we have

$$\alpha_{12}(x_1, x_2) = \begin{cases} \alpha_o & \text{for } (x_1, x_2) \in \tilde{\Gamma}_3^1, \\ \alpha_s & \text{for } (x_1, x_2) \in \Gamma_3^1 \setminus \tilde{\Gamma}_3^1. \end{cases}$$

The unknown parameters need to be estimated in this case are α_o, ϱ_1 and ς. The gradient of the objective function with respect to these new variables are easily obtained using the chain rule and the previous formulae. To avoid the dependence of the unknown parameters on their units and absolute values, we introduce the following dimensionless variable

$$v = \left(\frac{\varrho_1}{l_3}, \frac{\varsigma}{l_3}, \frac{\alpha_o}{\alpha_s} \right)'.$$

The estimation problem is subject to the constraints of the forms (26)–(28).

To make the estimation problem stable, we apply Tikhonov regularization technique. More precisely, we minimize the following objective functional

$$\mathcal{G}_1(v) = \mathcal{F}_h(\alpha) + \frac{1}{2}\gamma_1 \|v - v^*\|^2, \tag{29}$$

where v^* is an approximation of the desired solution. The regularization parameter γ_1 should be properly chosen for each particular problem.

4.2 Cylindrical object with the estimation of the cross section

In order to improve the estimation results of Step 1, in this step, we estimate the cross-section based on the estimation of the average values of the thermal diffusivity α_{12} on the horizontal cross-section of the soil volume across the object. To this end, we assume that the unknown parameters are $v(k_1, k_2) = \alpha_{12}^3(k_1, k_2)/\alpha_s$ (the factor $1/\alpha_s$ is used to transform the parameters to dimensionless ones), the dimensionless depth of burial ϱ_1/l_3, and the height ς/l_3. The average values $\alpha_{12}^1(k_1, k_2)$ and $\alpha_{12}^2(k_1, k_2)$ are approximated by

$$\begin{aligned} \alpha_{12}^1(k_1, k_2) &\simeq \frac{\alpha_s}{2}[v(k_1, k_2) + v(k_1 + 1, k_2)], \\ \alpha_{12}^2(k_1, k_2) &\simeq \frac{\alpha_s}{2}[v(k_1, k_2) + v(k_1, k_2 + 1)]. \end{aligned}$$

With these approximations, we have

$$\begin{aligned} \frac{\partial \alpha_{12}^1(k_1, k_2)}{\partial v(k_1, k_2)} &= \frac{\partial \alpha_{12}^1(k_1, k_2)}{\partial v(k_1 + 1, k_2)} = \frac{\alpha_s}{2}, \\ \frac{\partial \alpha_{12}^2(k_1, k_2)}{\partial v(k_1, k_2)} &= \frac{\partial \alpha_{12}^2(k_1, k_2)}{\partial v(k_1, k_2 + 1)} = \frac{\alpha_s}{2}, \\ \frac{\partial \alpha_{12}^3(k_1, k_2)}{\partial v(k_1, k_2)} &= \alpha_s. \end{aligned}$$

The estimation problem is devoted to the reconstruction of the new vector V consisting of the matrix v, ϱ_1/l_3 and ς/l_3. The objective functional is given as follows

$$\mathcal{G}_2(V) = \mathcal{F}(\alpha) + \gamma_2 TV(\alpha_{12}), \tag{30}$$

where $TV(\alpha_{12})$ is the total variation of the thermal diffusivity α_{12}. The problem is also subject to the constraints of the forms (26), (27) and (28). Here we use the total variation regularization to preserve the discontinuity of the coefficient.

5 Numerical results

In this section, we illustrate the performance of the algorithms presented in the previous section with a set of simulated data. Keeping in mind the application to landmine detection, the input functions are taken similar to real conditions. A soil domain of $0.35\times0.35\times0.4$ (m^3) is considered and the time interval of analysis is chosen to be $t_e = 16$ (h) (from 8:00 till 24:00, this choice is based on analysis on the effect of the solar radiation on the soil temperature, see [25]). The discretization grid sizes are chosen as $h = (0.01, 0.01, 0.01)$ (m) and $\Delta t = 120$ (s) resulting in $35 \times 35 \times 41$ space grid points and 481 time steps. We note that due to the small sizes of landmines, the spatial grid sizes should not be chosen too large while, according to our numerical trials, the time step can be more freely chosen. The soil is simulated as sand with the thermal diffusivity $\alpha_s = 6.402 \times 10^{-7}$ m^2/s.

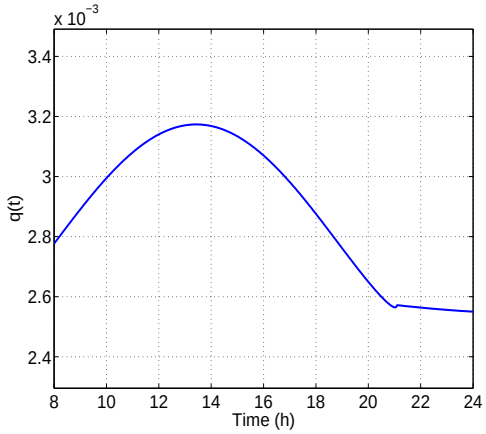

Figure 3: The boundary function $q(t)$.

The initial condition is uniform as $g(x) = 293$ (K) and the soil temperature at the bottom surface T_∞, which is assumed to be invariant in time, is set to be 293 (K) to make it consistent with the initial condition. The parameters p and $q(t)$ are calculated through weather conditions [27]. In this example, we have $p = 9.2272 \times 10^{-6}$ and $q(t)$ is depicted in Figure 3. Since the soil-surface heat flux is the source of thermal signatures, the soil-surface temperature contrast certainly depends on $q(t)$. This was confirmed by numerical simulations in [27]. As a consequence, the higher the heat flux, the deeper the object that could be detected.

In this work, we demonstrate the performance of the proposed algorithms with a circular cylindrical object of radius 0.03 m and height 0.05 m buried in the center of the soil domain at different depths. This object is of the same size as some anti-personnel mines [25]. Its

thermal properties are also given as of $2,4,6$-Trinitrotoluene (TNT — explosive) with $\alpha_o = 1.139 \times 10^{-7}$ m^2/s.

As mentioned in the introduction, in dealing with real experimental data, a chain of pre-processing steps must be applied for obtaining images representing the soil-surface apparent temperature. However, in this work, as the data is simulated, these pre-processing steps are not necessary. Instead, the measured data is given as the solution of the forward model. In order to avoid the so-called *inverse crime*, we use an explicit finite difference method to simulate the measured data. Then a random noise of magnitude of 0.1 K is added to the simulated data. This noise level should take into account both the temperature resolution of IR cameras and the model's error. We remark that the most important information in the measured data is the soil-surface temperature contrast between the object and the background, but not the temperature itself. This temperature contrast is generally small, say, less than a few degrees Kelvin (see Figures 4, 7 and 9(a)). Therefore, the noise level of 0.1 K is large in this situation, especially when the object is deeply buried.

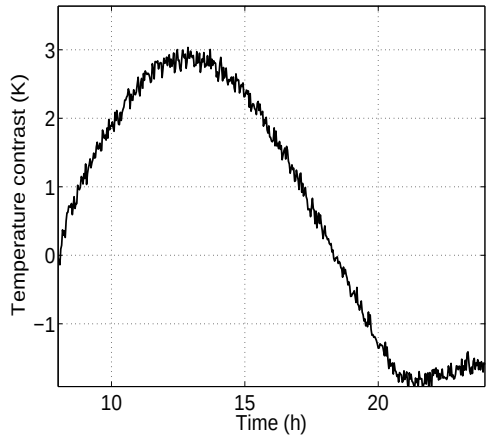

Figure 4: Measured temperature contrast of Example 5.1.

Example 5.1. We start the numerical demonstration with the case that the object is buried at 0.01 m. The noisy measured soil-surface temperature contrast, which is the difference between the soil-surface temperature above the object and that of the background, is depicted in Figure 4.

The exact dimensionless parameter vector in Step 1 is $v^e = (0.025, 0.125, 0.18)'$. We start the algorithm of Step 1 at the initial guess $v^0 = (0.1, 0.1, 0.9)'$. The regularization parameter is empirically chosen $\gamma_1 = 1$ by 'trial-and-error' tests. The approximation of the solution in the regularization term is chosen as $v^* = (0.05, 0.1, 0.2)'$ and the bound constraints

$$\alpha^l = 0.064 \times 10^{-7}, \quad \alpha^u = 6.402 \times 10^{-7},$$
$$\varrho_1^l = 0.001, \quad \varrho_1^u = 0.1, \quad \varsigma^u = 0.06.$$

That means, the height of the object is assumed to be between 0.01 and 0.06 (m). This choice is based on the analysis on the effect of the height on the soil-surface temperature mentioned in the beginning of this section.

In Step 1, the cross-section of the object is estimated using an anomaly detection technique that was presented in [29, 25]. The estimated cross-section is depicted in Figure 5(a). The figure shows that the estimated cross-section is a bit larger than the true one which is represented by the circle.

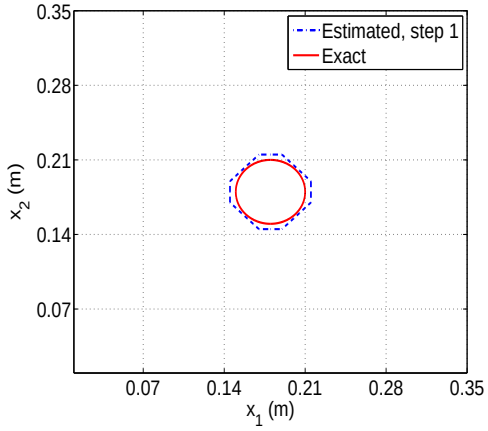

(a) Estimated cross-section in Step 1

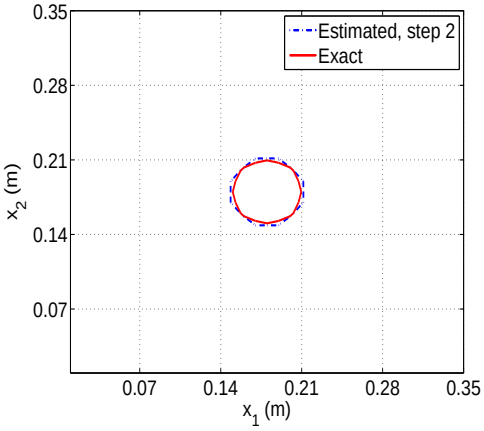

(b) Estimated cross-section in Step 2

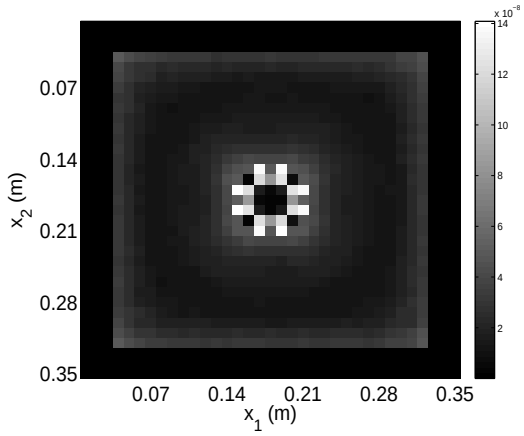

(c) Error of α_{12} in Step 2

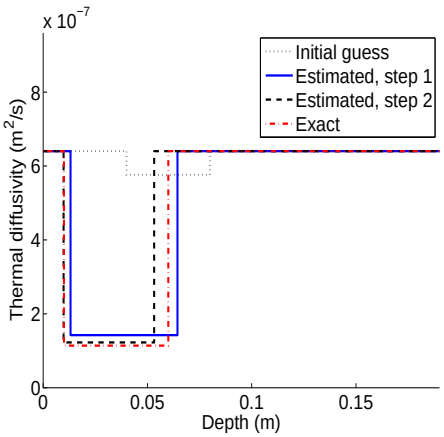

(d) Distribution of the coefficient in depth

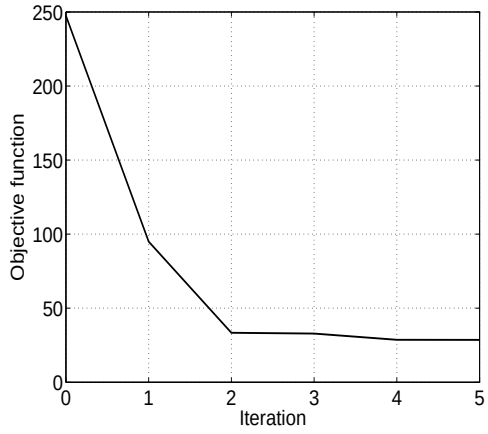

(e) Objective function of Step 1

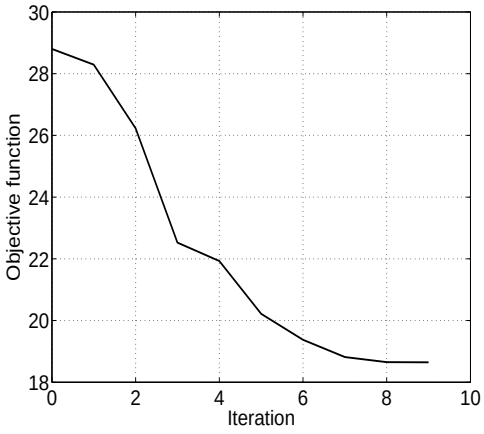

(f) Objective function of Step 2

Figure 5: Result of Example 5.1. Depth of burial = 0.01 m.

Figure 5(b) shows the estimated cross-section in Step 2. This cross-section was drawn based on the estimated values of α_{12}. The estimation error of α_{12} is shown in Figure 5(c). The estimated values of the thermal coefficient, the depth and the height of the object in both steps are depicted in Figure 5(d) in which we plot the distribution of the coefficient in depth. Note that the discontinuous points represent the upper (the depth of burial) and lower surfaces of the object (the height is the distance between the discontinuities). The figure indicates that, although we start the algorithm of Step 1 far from the true values, it still provides a quite good estimate of the coefficient. We recall that in this test, the height is constrained to be between 0.01 and 0.06 m. In Step 2, the result of Step 1 is used as the initial guess. The regularization parameter γ_2 is also empirically chosen to be 10^{-2}. As shown in Figure 5(b), the estimates for the depth and the thermal diffusivity of Step 2 are improved in comparing to the result of Step 1. However, the estimate of the height is less accurate. This again confirms that the effect of the object's height on the soil-surface temperature is not as strong as other parameters do.

We should emphasize that, due to the small number of unknowns, Step 1 converges very fast even we start the iterations far from the exact solution, see Figure 5(e), say, the objective functional decreases dramatically in the first two iterations. The algorithm of Step 2 also converges quickly thanks to the good initial guess provided by Step 1, see Figure 5(f).

Apart from the advantage of having a small number of unknowns in Step 1, the accurate result of Step 1 shown above is also due to the good estimate of the cross-section of the object as shown in Figure 5(a). In order to answer the question if we still can accurately reconstruct the coefficient when the cross-section is not really accurately estimated, we show in Figure 6 the results of both steps for another estimated cross-section. The figure shows that, due to the larger estimated cross-section, the diffusivity of the object is not accurately reconstructed by Step 1. However, the result of Step 2 is much better as shown in Figure 6(d). We also can see from Figure 6(a)-(c) that the cross-section is improved in Step 2. This confirms the ability of Step 2 to improve results of Step 1 when the cross-section is not accurately reconstructed by anomaly detection algorithms. Of course, due to the less accurate result of Step 1, more iterations were needed to obtain an accurate estimate.

Example 5.2. It is natural that the deeper the object is buried, the more difficult to detect and characterize it. To show the performance of the proposed algorithms for objects buried at deeper depths, we now consider the case in which the same object is buried at the depth of 0.03 m. The measured soil-temperature contrast is plotted in Figure 7. All the parameters are the same as in the previous example.

We start Step 1 at the initial guess $v^0 = (0.05, 0.1, 0.9)'$. The estimated cross-section used in this step is depicted in Figure 8(a). The results of both steps are shown in Figure 8.

It is clear from the figure that the result of this example is not as good as the previous one, but it is still reasonably good. We note that, as shown in Figure 7, the magnitude of the measured soil-surface temperature contrast in this case is much smaller than in the previous example. Therefore, it is understandable that the estimate in this example is less accurate compared to the previous example.

Example 5.3. The above examples show that the accuracy of the estimates depends on the depth at which the object is buried. Of course, it is impossible to detect an object which does not show any signal (contrast) in the measured data. To show this, we consider the case when the object is buried at 0.08 m. Figure 9 show that the algorithms of the two steps fail to estimate the coefficient even when we start the iterations from a good initial guess in Step 1. It is clearly

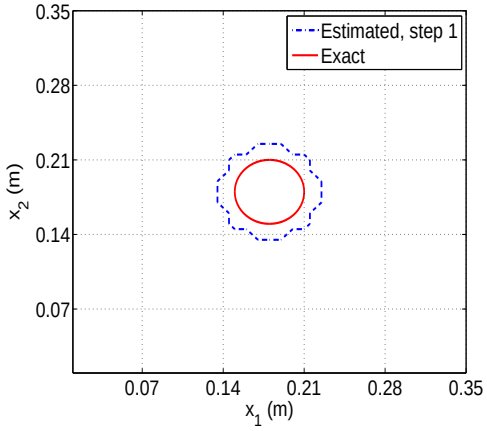

(a) Estimated cross-section in Step 1

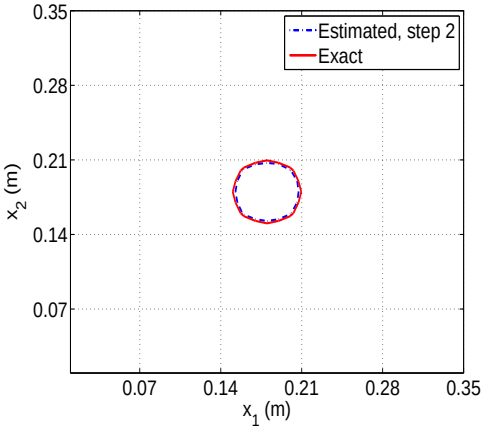

(b) Estimated cross-section in Step 2

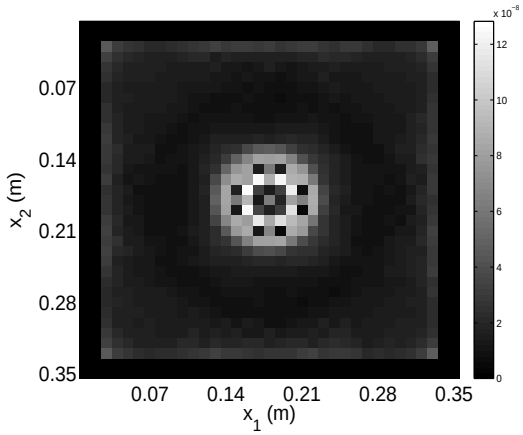

(c) Error of α_{12} in Step 2

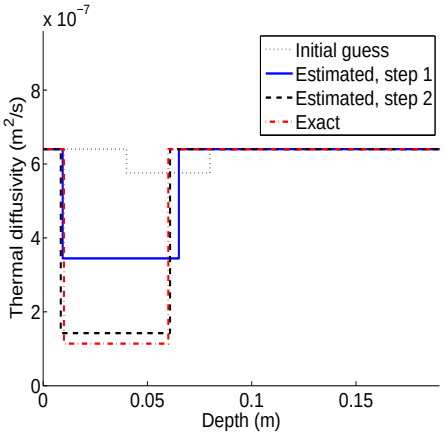

(d) Distribution of the coefficient in depth

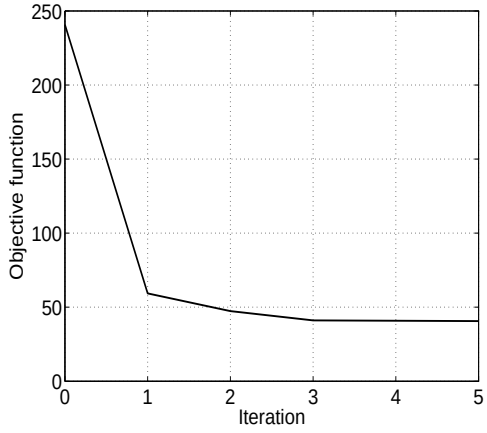

(e) Objective function of Step 1

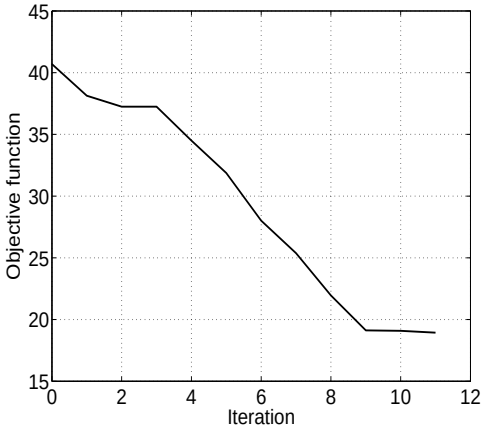

(f) Objective function of Step 2

Figure 6: Result of Example 5.1 for a different estimated cross-section.

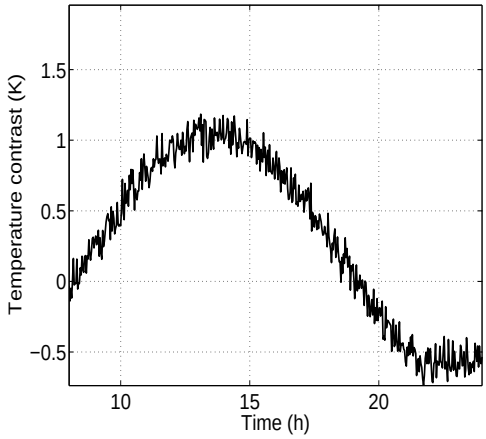

Figure 7: Measured temperature contrast of Example 5.2.

due to the fact that the noisy measured temperature contrast is just a bit higher than the noise level.

Example 5.4. Finally, let us test the algorithm with a parallelepiped of the sizes $0.07 \times 0.04 \times 0.05$ (m^3) located at the center of the soil domain and buried at 0.01 m. In this case, the cross-section of the object is rectangular. For this object, we start the algorithm at the same initial guess as in Example 5.1. The estimation results of the two steps are depicted in Figure 10.

It is clear from the figure that, the image segmentation technique only provides a very rough estimate of the cross-section of the object. Therefore, the result of Step 1 is not really good (Figure 10(a)). The advantage of Step 2 is again confirmed because it can improve both the estimation of the cross-section, see Figure 10(b), and the distribution of the thermal diffusivity in depth, see Figure 10(d).

6 Conclusion

We introduced the inverse problem setting for buried object detection. The problem was stated as a least-squares minimization problem. The existence of a solution to this problem was given in the space of functions of bounded variation.

In solving the inverse problem, we made use of quasi-Newton trust region method with the adjoint technique for calculating the gradient of the objective functional. The adjoint technique was not directly applied to the continuous inverse problem, but to the discretized one. This approach enables calculating the exact gradient of the discrete objective functional.

In dealing with the inverse problem, we realized that the problem is extremely ill-posed. In this work, to reduced the ill-posedness of the problem, emphasizing the application to anti-personal landmine detection, we assumed that the objects are (not necessarily circular) cylindrical and made use of a two-step method. In the first step, we use image segmentation techniques to detect the presence of anomalies and derive rough estimates of their horizontal cross sections. Then the inverse problem is reduced to estimate only three parameters: the depth of burial, the height and the thermal diffusivity of each detected anomaly. In the second step, for improving the result of the first step, we use this result as an initial guess to estimate the depth of burial, the height and mean values of the thermal diffusivity on a horizontal cross-section of the soil domain across the buried object.

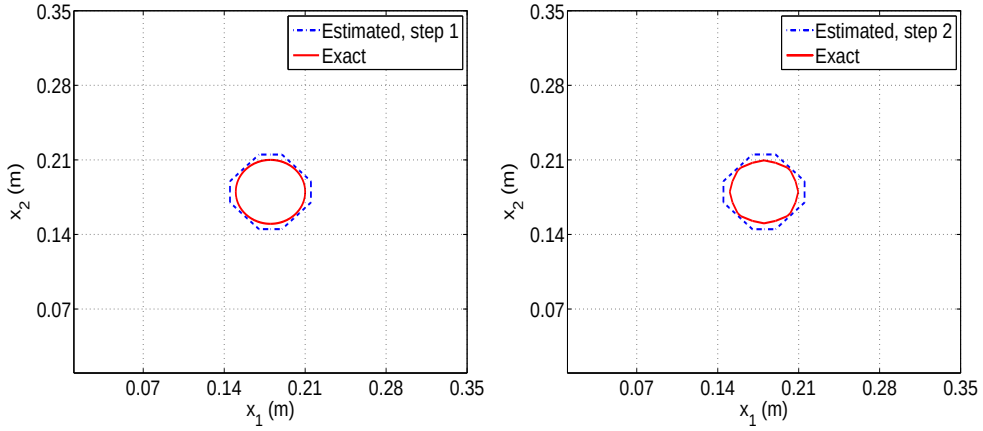

(a) Estimated cross-section in Step 1

(b) Estimated cross-section in Step 2

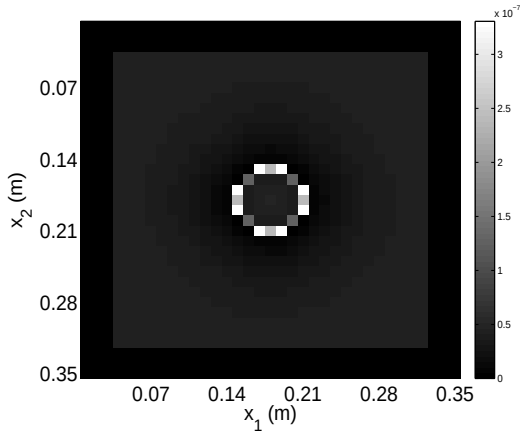

(c) Error of α_{12} in Step 2

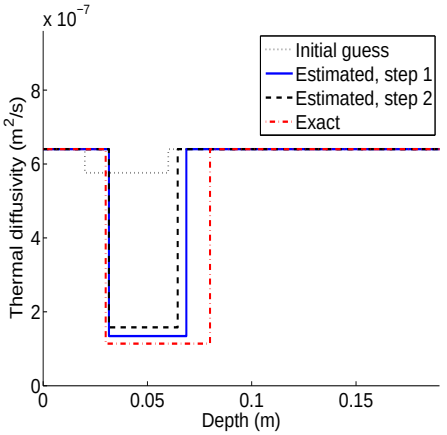

(d) Distribution of the coefficient in depth

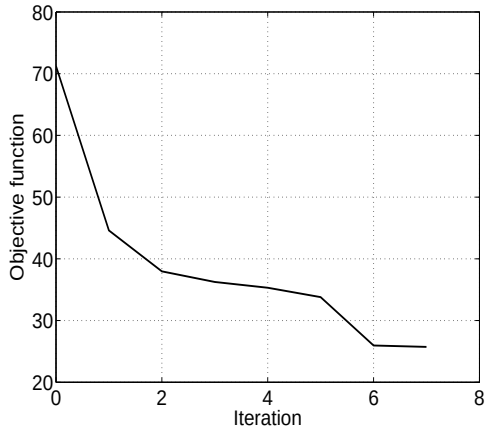

(e) Objective function of Step 1

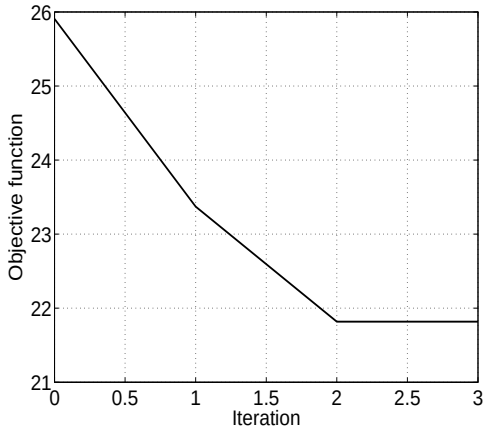

(f) Objective function of Step 2

Figure 8: Result of Example 5.2. Depth of burial = 0.03 m.

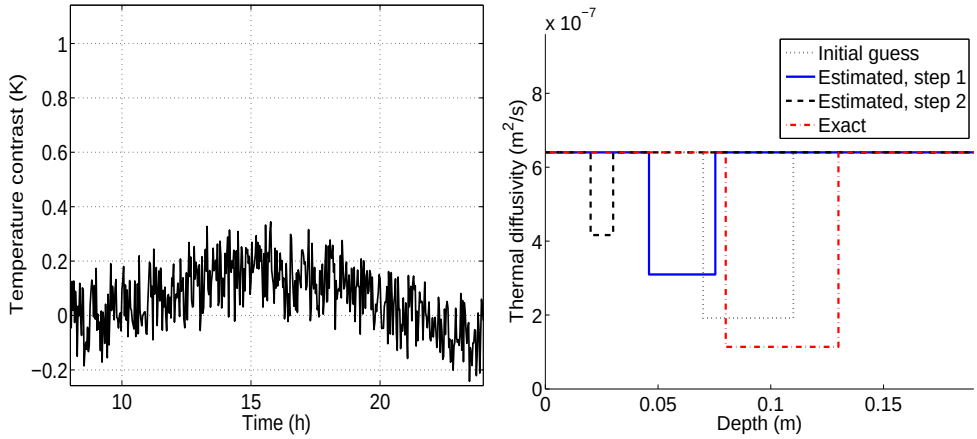

(a) Measured temperature contrast (b) Distribution of the coefficient in depth

Figure 9: Result of Example 5.3. Depth of burial = 0.08 m.

The numerical examples show the potential of the proposed methods. The results also confirm a natural phenomenon that the deeper the object is buried, the less accurate the reconstruction is. The numerical results showed good reconstruction results with shallowly buried objects. However, the reconstruction is less accurate with the objects buried at deep depths. This is one of the limitations of IR thermography which makes it to be referred to as a *boundary technique*. More numerical results presented in [25, 29] also showed that the larger the object is, the more accurate the reconstruction is.

The proposed inversion method in this work was confined to only upright cylindrical objects. As future work, to enhance the practicality of the method, more general types of shapes should be considered. It would be also interesting to tackle inhomogeneous soil and objects. Other shape parametrization methods are also being investigated and the results will be reported in a future publication.

Acknowledgments

The authors are grateful to the Associate Editor and the referees for their corrections and suggestions for improving the paper. The work was partly done when N.T. Thành and D.N. Hào were with Department of Electronics and Informatics, Vrije Universiteit Brussel. The work of D.N. Hào was supported in part by NAFOSTED Grant 101.01.22.09.

References

[1] H. Banks. Computational issues in parameter estimation and feedback control problems for partial differential equatioins. *Physica D*, 60:226–238, 1992.

[2] C.-B. Chung and C. Kravaris. Identification of spatial discontinuous parameters in second-order parabolic systems by piecewise regularisation. *Inverse Problems*, 4(4):973–994, 1988.

[3] T. F. Coleman and Y. Li. An interior trust region approach for nonlinear minimization subject to bounds. *SIAM Journal on Optimization*, 6(2):418–445, 1996.

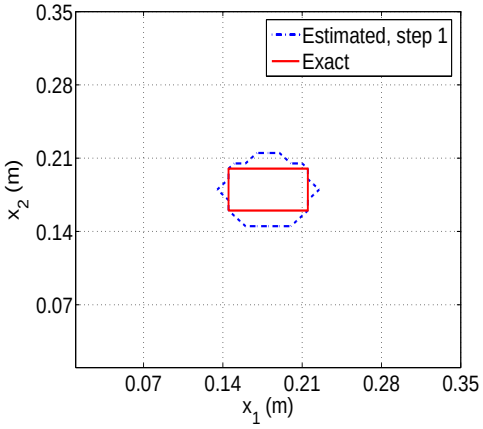

(a) Estimated cross-section in Step 1

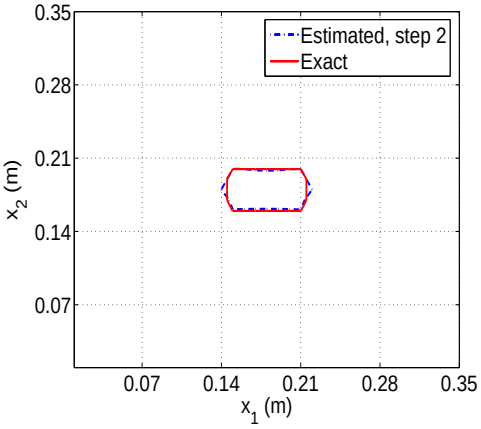

(b) Estimated cross-section in Step 2

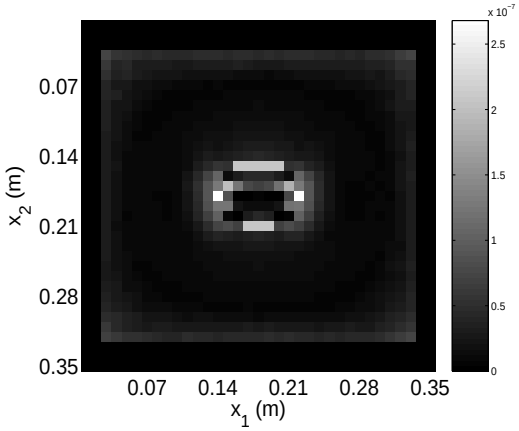

(c) Error of α_{12} in Step 2

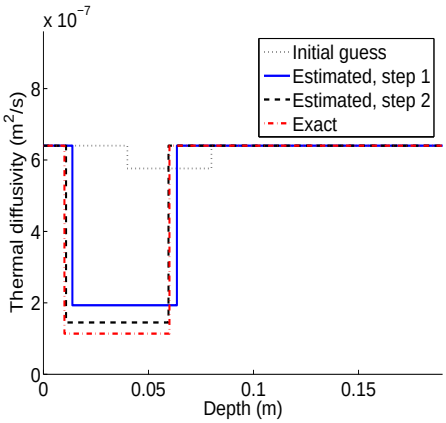

(d) Distribution of the coefficient in depth

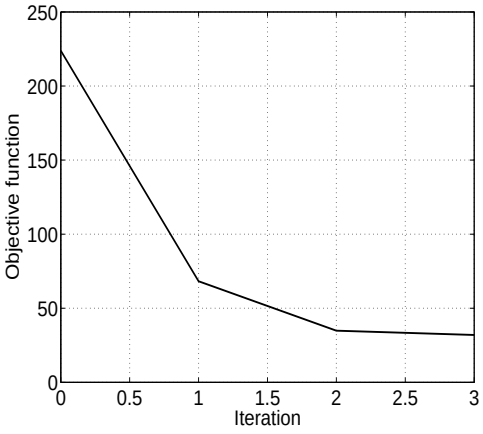

(e) Objective function of Step 1

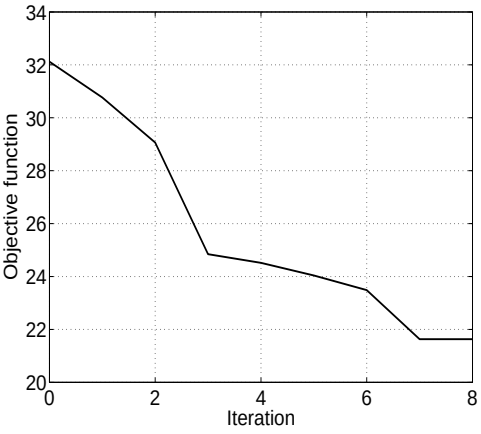

(f) Objective function of Step 2

Figure 10: Result of Example 5.4. Depth of burial = 0.01 m.

[4] F. Cremer, N. T. Thành, L. Yang, and H. Sahli. Stand-off thermal IR minefield survey, system concept and experimental results. In R. S. Harmon, J. T. Broach, and J. H. Holloway, Jr., editors, *Proceedings of SPIE 5794, Detection and Remediation Technologies for Mine and Minelike Targets X*, pages 209–220, 2005.

[5] O. Dorn, E. L. Miller, and C. M. Rappaport. A shape reconstruction method for electromagnetic tomography using adjoint fields and level sets. *Inverse Problems*, 16(5):1119–1156, 2000.

[6] P. Duchateau, R. Thelwell, and G. Butters. Analysis of an adjoint problem approach to the identification of an unknown diffusion coefficient. *Inverse Problems*, 20(2):601–625, 2004.

[7] A. Elayyan and V. Isakov. On uniqueness of recovery of the discontinuous conductivity coefficient of a parabolic equation. *SIAM Journal on Mathematical Analysis*, 28(1):49–59, 1997.

[8] E. Giusti. *Minimal Surfaces and Functions of Bounded Variation*, volume 80 of *Monographs in Mathematics*. Birkhäuser Verlag, Basel, 1984.

[9] S. Gutman. Identification of discontinuous parameters in flow equations. *SIAM J. Control Optim.*, 28(5):1049–1060, 1990.

[10] S. Gutman and J. Ha. Identifiability of piecewise constant conductivity in a heat conduction process. *SIAM J. Control Optim.*, 46(2):694–713, 2007.

[11] S. Gutman and J. Ha. Parameter identifiability for heat conduction with a boundary input. *Math. Comput. Simulation*, 79(7):2192–2210, 2009.

[12] N. S. Hoang and A. G. Ramm. An inverse problem for a heat equation with piecewise-constant thermal conductivity. *J. Math. Phys.*, 50(6):063512, 2009.

[13] Y. L. Keung and J. Zou. Numerical identifications of parameters in parabolic systems. *Inverse Problems*, 14(1):83–100, 1998.

[14] K. Khanafer, K. Vafai, and B. A. Baertlein. Effects of thin metal outer case and top air gap on thermal IR images of buried antitank and antipersonnel land mines. *IEEE Transactions on Geoscience and Remote Sensing*, 41(1):123–135, 2003.

[15] C. Kravaris and J. H. Seinfeld. Identification of parameters in distributed parameter systems by regularization. *SIAM J. Control Optim.*, 23(2):217–241, 1985.

[16] K. Kunisch and L. White. The parameter estimation problem for parabolic equations and discontinuous observation operators. *SIAM J. Control Optim.*, 23(6):900–927, 1985.

[17] P. K. Lamm. Estimation of discontinuous coeffcients in parabolic systems: applications to reservoir simulation. *SIAM J. Control Optim.*, 25(1):18–37, 1987.

[18] J. L. Lions. *Optimal Control of Systems governed by Partial Differential Equations*. Springer-Verlag, Berlin, 1971.

[19] P. López. *Detection of Landmines from Measured Infrared Images using Thermal Modelling of the Soil*. PhD Thesis, University of Santiago de Compostela, 2003.

[20] G. I. Marchuk. Splitting and alternating direction methods. In P. G. Ciaglet and J. L. Lions, editors, *Handbook of Numerical Mathematics. Volume 1: Finite Difference Methods.* Elsevier Science Publisher B.V., North-Holland, Amsterdam, 1990.

[21] G. I. Marchuk. *Adjoint Equations and Analysis of Complex Systems.* Kluwer Academic Publishers, Dordrecht, 1995.

[22] The Math Works Inc. *Optimization Toolbox for Use with Matlab: User's Guide*, 3rd edition, 1990–2004.

[23] A. Muscio and M. A. Corticelli. Land mine detection by infrared thermography: reduction of size and duration of the experiments. *IEEE Transactions on Geoscience and Remote Sensing*, 42(9):1955–1964, 2004.

[24] S. J. Norton. Iterative inverse scattering algorithms: Methods of computing Frechet derivatives. *J. Acoust. Soc. Am.*, 106(5):2653–2660, November 1999.

[25] N. T. Thành. *Infrared Thermography for the Detection and Characterization of Buried Objects.* PhD Thesis, Vrije Universiteit Brussel, Brussels, Belgium, 2007.

[26] N. T. Thành, D. N. Hào, and H. Sahli. Infrared thermography for landmine detection. In R. I. Hammoud, editor, *Augmented Vision Perception in Infrared. Algorithms and Applied Systems*, pages 3–36. Springer, 2009.

[27] N. T. Thành, H. Sahli, and D. N. Hào. Finite difference methods and validity of a thermal model for landmine detection with soil property estimation. *IEEE Transactions on Geoscience and Remote Sensing*, 45(3):656–674, 2007.

[28] N. T. Thành, H. Sahli, and D. N. Hào. Estimation of piecewise constant coefficients of parabolic equations: applications to the detection of buried objects. *Inverse Problems in Science and Engineering*, 16(7):903–925, 2008.

[29] N. T. Thành, H. Sahli, and D. N. Hào. Infrared thermography for buried landmine detection: inverse problem setting. *IEEE Transactions on Geoscience and Remote Sensing*, 46(12):3987–4004, 2008.

[30] C. R. Vogel and J. G. Wade. Analysis of costate discretizations in parameter estimation for linear evolution equations. *SIAM J. Control Optim.*, 33(1):227–254, 1995.